Emergence of exchange bias and giant coercive field enhancement by internal magnetic frustration in La0.67Sr0.33MnO3 thin films

Ali Basaran, C. Monton, J. Trastoy, R. Bernard, K. Bouzehouane, J.E. Villegas, Ivan Schuller

▶ **To cite this version:**

Ali Basaran, C. Monton, J. Trastoy, R. Bernard, K. Bouzehouane, et al.. Emergence of exchange bias and giant coercive field enhancement by internal magnetic frustration in La0.67Sr0.33MnO3 thin films. Journal of Magnetism and Magnetic Materials, 2022, 550, pp.169077. 10.1016/j.jmmm.2022.169077 . hal-03864329

HAL Id: hal-03864329
https://cnrs.hal.science/hal-03864329v1

Submitted on 21 Nov 2022

HAL is a multi-disciplinary open access archive for the deposit and dissemination of scientific research documents, whether they are published or not. The documents may come from teaching and research institutions in France or abroad, or from public or private research centers.

L'archive ouverte pluridisciplinaire **HAL**, est destinée au dépôt et à la diffusion de documents scientifiques de niveau recherche, publiés ou non, émanant des établissements d'enseignement et de recherche français ou étrangers, des laboratoires publics ou privés.

Journal of Magnetism and Magnetic Materials 550 (2022) 169077

Contents lists available at ScienceDirect

Journal of Magnetism and Magnetic Materials

journal homepage: www.elsevier.com/locate/jmmm

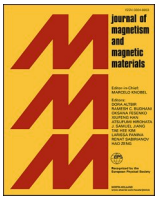

Emergence of exchange bias and giant coercive field enhancement by internal magnetic frustration in $La_{0.67}Sr_{0.33}MnO_3$ thin films

Ali C. Basaran [a,*], C. Monton [a,b], J. Trastoy [c], R. Bernard [c], K. Bouzehouane [c], J.E. Villegas [c], Ivan K. Schuller [a]

[a] Department of Physics and Center for Advanced Nanoscience, University of California San Diego, La Jolla, CA 92093, USA
[b] General Atomics, P.O. Box 85608, San Diego 92186, USA
[c] Unité Mixte de Physique, CNRS, Thales, Université Paris-Saclay, 91767 Palaiseau France

ARTICLE INFO

Keywords:
Exchange Bias
Coercive field enhancement
Ion bombardment
LSMO thin films

ABSTRACT

We have studied the influence of controlled defects on the magnetic properties of $La_{0.67}Sr_{0.33}MnO_3$ (LSMO) thin films. We used 100 nm thick epitaxial LSMO films, which were grown on $SrTiO_3$ substrates and introduced stoichiometry changes and defects using oxygen ion irradiation through nanoporous alumina masks. Oxygen irradiation through the mask creates cascades of defects in spatially-modulated regions in the plane of the LSMO film. The magnetic properties of the samples were compared before and after the irradiation. We have found that irradiation reduces the ferromagnetic ordering temperature, decreases the total magnetization, enhances the coercivity, and induces exchange bias below 50 K. The coercivity enhancement is dramatically higher below 50 K and can be associated with exchange bias. These results can be explained by the formation of Mn-rich antiferromagnetic or ferrimagnetic phases within the bombarded regions that are exchange coupled to the non-irradiated - ferromagnetic host.

1. Introduction

Structural defects and stoichiometry play a crucial role in determining the physical properties of thin-film perovskite manganites. In particular, $La_{1-x}Sr_xMnO_3$ (LSMO) exhibits a broad range of physical phenomena such as metal–insulator transition, ferromagnetism, and colossal magnetoresistance [1,2]. In general, epitaxial LSMO thin films on $SrTiO_3$ substrates show a paramagnetic to ferromagnetic transition above 300 K. This transition close to room temperature makes them suitable for many potential spintronics applications [3,4]. However, the magnetic phase diagram of LSMO films strongly depends on the La, Sr, and O concentrations [5], strain [6], or geometry [7]. The characteristic magnetic properties of LSMO films, including their magnetic transition temperature, are mostly ascribed to film thickness, strain, structural defects, and intergranular structure [6,8–10]. Moreover, manganites are intrinsically inhomogeneous caused by strong tendencies toward phase separation into inhomogeneous magnetic phases which give rise to significant effects such as colossal magnetoresistance [11]. Therefore, inducing controlled inhomogeneous magnetic phases by nano-modulating the sample with structural and stoichiometric defects could lead to new spintronic applications [12].

Phase inhomogeneities can be induced by localized ion irradiation to create controlled defects [13] which modify the electronic [14,15] and magnetic properties [16–18] of perovskite thin films. In general, the magnetic changes originate from structural modifications that can be controlled by the irradiation ion element, dose, and energy [19,20]. Furthermore, lateral magnetic patterning becomes feasible by combining ion irradiation with various lithographical techniques [15,21], such as self-assembled nanosphere lithography [22] and photolithography. However, most of these lithography techniques are not cost effective, require thermal or chemical post-treatments that can affect samples, and can only be applied in a relatively small area. To this end, anodic aluminum oxide (AAO) nanoporous membranes with self-organized arrays of nano-holes can be used as an irradiation mask to locally modify the physical properties of nanometer-sized regions. Large area (cm^2) AAO membranes are simple to manufacture. The anodization technique allows precise control of the pore diameter and interpore distance to obtain sub 100 nm pitch size [23]. Lower aspect ratio membranes permit the irradiation ions to reach the sample without colliding with the walls. Hence, a combination of ion irradiation and

* Corresponding author.
E-mail address: abasaran@physics.ucsd.edu (A.C. Basaran).

https://doi.org/10.1016/j.jmmm.2022.169077
Received 23 October 2021; Received in revised form 15 January 2022; Accepted 18 January 2022
Available online 21 January 2022
0304-8853/© 2022 The Authors. Published by Elsevier B.V. This is an open access article under the CC BY license (http://creativecommons.org/licenses/by/4.0/).

AAO mask can be used to create inhomogeneous magnetic phases through controlled structural or stoichiometric defects.

Irradiation at well-defined regions may alter the exchange anisotropies between irradiated and non-irradiated areas that may result exchange bias [24]. Exchange bias between ferromagnetic and antiferromagnetic layers arises from the unidirectional anisotropy induced at the interface between these two layers [25,26]. In some cases, exchange bias is found in artificially modulated single ferromagnetic thin films [27] or ferromagnet/spin glass systems [28]. Many studies imply that defects in the ferromagnetic layer affect the reversal mechanism, enhance the coercive field, and can induce exchange bias. However, a clear correlation between the nature of defects and its effects on the magnetic properties is not known [29].

The aim of this work is to present a systematic study of the effects induced by controlled 2 dimensional defects on the magnetic properties of LSMO manganite thin films. To this end, we use AAO membranes as a mask through which we perform oxygen ion (O^+) irradiation to induce localized defects in the plane and which modify the magnetic properties of the LSMO thin films. Energetic ions reaching the manganite thin film through the pores induce structural and chemical disorder locally, replicating the nanoscale pattern of the AAO mask. A comparison of the magnetic properties of LSMO thin films before and after the irradiation for various irradiation doses is presented.

2. Experimental

100 nm $La_{0.67}Sr_{0.33}MnO_3$ (LSMO) epitaxial thin films were grown on a 10 mm × 10 mm $SrTiO_3$ (STO) substrate by pulse laser deposition. The growth was done at T = 700 °C in oxygen pressure p = 0.2 mbar using a KrF 248 nm excimer laser with an energy density of ~1 J cm^{-2} and a repetition rate of 15 Hz. Optimum oxygenation was ensured by increasing the oxygen pressure to 800 mbar before cooling down to room temperature. The sample was cut into ~5 mm × 5 mm pieces to obtain 4 identical - as grown - samples. A 300 nm thick porous alumina (AAO) mask was prepared by anodizing high-purity aluminum sheets using the two-step anodization method and transferred on LSMO film pieces using the transferring method described in Ref. [30]. The sample preparation steps are illustrated in Fig. 1(a–d). The quality of the resulting porous membrane was checked by scanning electron microscopy (Fig. 1e). The average pore size was found to be around 70 nm with 110 nm interspacing between the pores. After masks were placed on LSMO films, the samples were irradiated with 110 keV oxygen ions at several doses on the order of 10^{14} ions/cm^2.

The magnetic characterizations were performed in a Quantum Design DynaCool system equipped with a 9 T superconducting magnet and a vibrating sample magnetometer. Samples were mounted on a quartz paddle using Kapton tape and placed into the chamber in such a way that the applied magnetic field was oriented parallel to the film plane. The AAO mask was left on the LSMO samples since it is diamagnetic and does not affect the magnetic behavior of the LSMO film. The superconducting magnet is demagnetized from 5 T before each measurement cycle in order to obtain the minimum possible remnant magnetization that is typically less than ±5 Oe in our system.

3. Results

In order to ascertain the location of vacancies created by the irradiation, we have used the transport of ions in matter (TRIM) program from stopping and range of ions in matter (SRIM) [31]. From these simulations the depth profile of irradiated ions and created vacancies into the manganite films were calculated (not shown). While in the exposed areas the damage is around 3.4 vacancies/ion in the LSMO, in

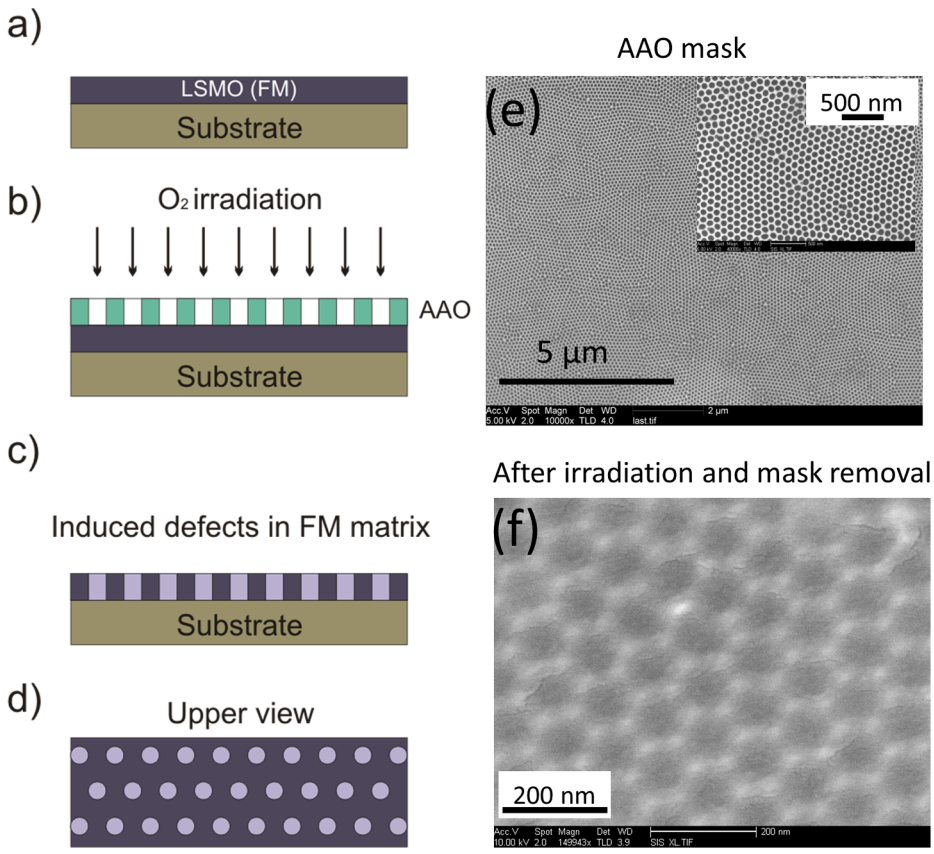

Fig. 1. (a–d) Sketch of the sample fabrication steps. (e) SEM image of the AAO mask transferred onto the LSMO sample and (f) after oxygen ion irradiation and mask removal. The contrast between dark and light regions is due to the changes in the conductivity and corresponds to the irradiation effect that resembles the honeycomb structure of the AAO mask.

the masked areas the damage is just about 0.01 vacancy/ion. Furthermore, vacancy creation in the masked areas was concentrated on the surface where the maximum density is 2.5×10^{-5} vacancies/(ion-angstrom), while in the exposed areas the minimum density found to be 2×10^{-3} vacancies/(ion-angstrom). We can conclude that there is at least two order-of-magnitude difference in vacancy creation between exposed and masked areas. Therefore, oxygen ions reach the LSMO film through the holes and create defects, which lead to changes in the magnetic and electronic properties in laterally confined regions. The SEM image after AAO mask removal shows the irradiated areas have different contrast (dark regions) and the honeycomb structure of AAO was successfully transferred on the samples (Fig. 1(f)). A small difference in the contrast between edges and vertices of the hexagons in the honeycomb structure could be due to stronger bonds at the vertices that further reduces the ion penetration into the LSMO layer.

To explore the magnetic behavior of the LSMO thin films, the temperature dependence of field cooled (FC) magnetization in an external field of 1 kOe was recorded. 1 kOe cooling field was chosen to assure that the applied field is high enough to be in the saturation regime. The magnetization of an as-grown sample increases rapidly at the transition temperature close to 335 K, which suggests FM correlation of the spins (Fig. 2a, black squares). We employed the same experimental protocol after both AAO mask transfer and oxygen ion irradiation. It is important to note that the AAO mask transferring decreases the magnetization of the samples without changing the ferromagnetic ordering temperature (Fig. 2a, red circles). 2×10^{14} ions/cm^2 oxygen irradiation through the holes further decreases the magnetization as well as lowers the ferromagnetic ordering temperature to 283 K (Fig. 2a, blue triangles). Similar temperature dependence of magnetization in correlation with irradiation doses appears for all measured samples (Fig. 2b). The magnetization and transition temperatures significantly decrease as irradiation dose increases and the transition occurs over a much broader range of temperatures.

Hysteresis loops were measured at different temperatures both before and after the irradiation to investigate the ion irradiation effect on magnetization reversal. Fig. 3 shows hysteresis loops at four different temperatures. Hysteresis loops were recorded by scanning the magnetic field starting from positive to negative saturation direction. The data have been corrected for a linear diamagnetic slope from the substrate. Coercive field values were calculated from the average of positive and negative applied fields where magnetization crosses zero. Fig. 3(a) shows hysteresis loops of sample S1 after AAO mask transfer at four different temperatures before the irradiation. As the temperature decreases, the coercive field increases while the saturation magnetization changes according to the typical temperature dependence, which is small compared to the post-irradiation situation. Fig. 3b shows hysteresis loops of the same sample after 2×10^{14} ions/cm^2 irradiation. After irradiation, both the saturation magnetization and the coercive field increase remarkably as the temperature decreases. At 5 K, a giant coercive field enhancement (from 26 to 431 Oe) appears that is not expected from a simple temperature dependence of a ferromagnet. This giant coercive field enhancement only appears after the irradiation and

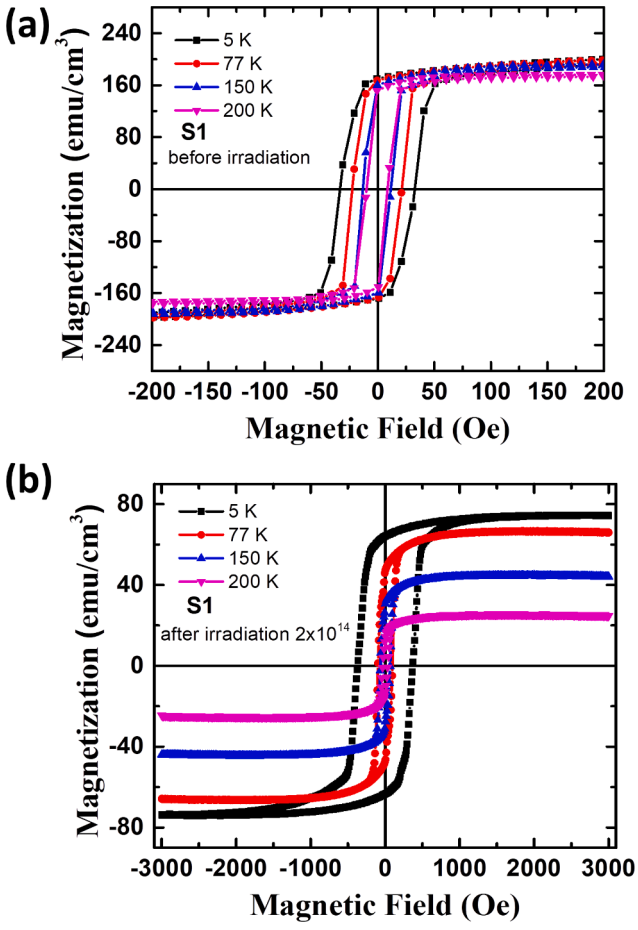

Fig. 3. Selected hysteresis curves at different temperatures for LSMO samples masked with AAO. (a) Before and (b) after 2×10^{14} oxygen ion irradiation dose for the same sample S1.

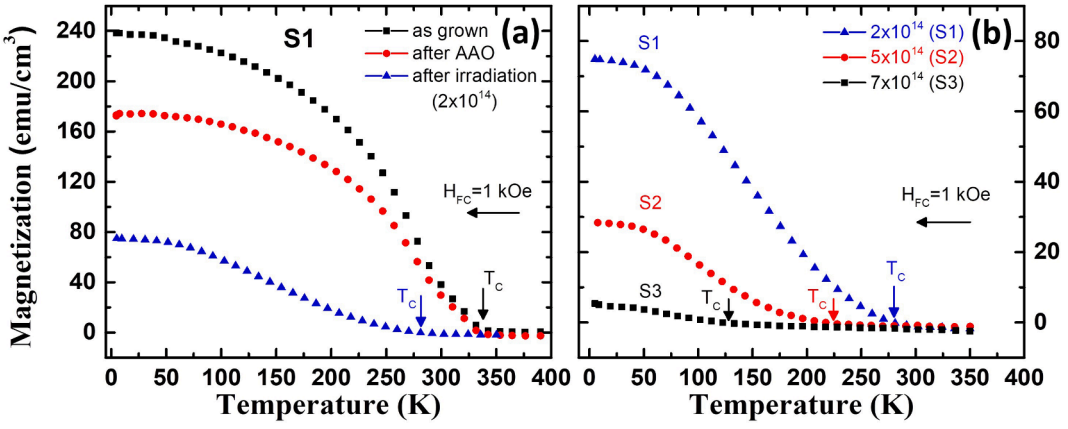

Fig. 2. (a) Temperature dependence of the saturation magnetization of as grown sample (black), after AAO mask transfer (red), and after 2×10^{14} ions/cm^2 oxygen irradiation (blue). The data was taken with 1 kOe field cooling. (b) Similar temperature dependence of the saturation magnetization for three different irradiation doses. Note that the ferromagnetic ordering temperature (Tc) is decreasing with increasing irradiation dose as indicated by arrows. (For interpretation of the references to color in this figure legend, the reader is referred to the web version of this article.)

thus it is apparently induced by the oxygen irradiation in our experiment.

Hysteresis curves were measured after 1 kOe field cooling using the same experimental protocol for all samples. In all cases, the coercive field increases by decreasing the temperature. Fig. 4 shows change in the coercive fields as a function of temperature for three different irradiation doses. Measurement of an as-grown sample is also included for comparison. All samples have similar coercive fields at high temperatures. As the temperature decreases the change in the coercive fields differ for different irradiation doses. Below 50 K a large coercive field enhancement appears only for irradiated samples. For the highest irradiated dose sample (7×10^{14} ions/cm^2) at 5 K, the coercive field is 1346 Oe, which corresponds to an enhancement of more than 50 times when compared to the 25 Oe of the same as-grown sample, or the 33 Oe measured after the AAO transfer (not shown). The dependence of coercive fields on irradiation dose at 5 K is plotted in the inset. The change in the coercive field is almost linear dependent on the irradiation up to the highest irradiation dose (7×10^{14} ions/cm^2) used in our experiment. This demonstrates that the coercive field enhancement is induced by the irradiation.

Fig. 5 shows hysteresis loops for irradiated samples at three different doses. Besides the large coercive field enhancement due to the irradiation, an apparent negative horizontal loop shift was observed after 1 kOe field cooling to 5 K. The observed exchange bias for the highest irradiation dose (7×10^{14} ions/cm^2) sample corresponds to 151 Oe (Fig. 5c). Applying the same experimental protocol to other samples reveals that the exchange bias field is decreasing with decreasing irradiation dose and disappears for non-irradiated samples. The dependence of the induced exchange-bias field to irradiation dose is included in the inset of Fig. 4. For an easy comparison, the evolution of coercive fields, exchange-bias fields and magnetizations are given in Table 1.

4. Discussion

After placing the AAO mask on as-grown films, samples were irradiated with 110 keV oxygen ions with doses 2×10^{14}, 5×10^{14}, and 7×10^{14} ion/cm^2. Based on SRIM we have chosen a 100 nm film thickness so that the 110 keV ions produce a constant damage profile across the film. The estimated depth range is 200–300 nm in these conditions. On the other hand, damage distribution in lateral was confined by the AAO mask. The SEM image after irradiation and mask removal in Fig. 1 suggests the AAO pattern is successfully transferred on the LSMO films.

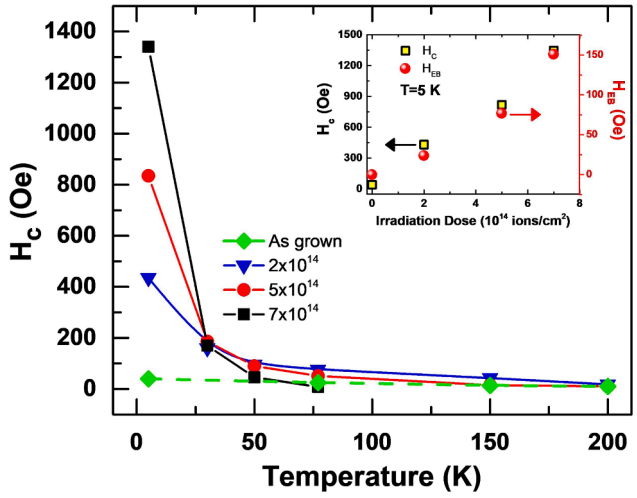

Fig. 4. Temperature dependence of the coercive fields for different irradiation doses. As grown sample is included for comparison. Lines in the figure are guide for the eye. The inset shows coercive field and exchange bias dependence on the irradiation dose after 1 kOe FC at 5 K.

The imprinted honeycomb structure, which appears as dark and bright regions, is produced by the electronic contrast of the different conducting regions. Ion irradiation creates defects and increases the disorder within the conducting regions that results the conductivity of patterned areas were strongly degraded and correspond to darker regions in SEM [32]. Similar nano-patterning approach using porous anodic alumina mask and ion irradiation is widely used in the literature [33,34].

Since there are two separate processes, the mask transfer and ion irradiation, involved in nano-pattern imprinting using the AAO mask, we investigated the differences on magnetization behavior after each. (i) After the AAO mask transfer, the decrease in the magnetization (Fig. 2a) and coercive field (not shown) indicates that LSMO films are naturally sensitive to the chemicals used during the mask transfer protocol. However, compared to values after irradiation, these changes are relatively small and do not modify the hysteresis shape, which suggests the reversal mechanism is still the same. In other words, the chemicals used during the AAO mask transfer could affect the magnetic moments near the film surface, however they do not reach deep in the film and affect the overall magnetization reversal. (ii) After irradiation, a large decrease in the magnetization is found (Fig. 2b) corresponding to applied irradiation doses (up to 98% for 7×10^{14} ions/cm^2). In addition to the magnetization decrease, the ferromagnetic ordering temperature (T_C) lowers (Fig. 2b) to 283, 223, and 123 K for 2×10^{14}, 5×10^{14}, and 7×10^{14} ions/cm^2 irradiation, respectively. The ferromagnetic transition temperature, accompanied with an insulator–metal transition, decreases with increasing structural and oxygen site defects that can be introduced either controlling conditions during the film growth or by post growth ion irradiation [35–37]. Furthermore, coercive fields dramatically enhance, up to 1346 Oe for 7×10^{14} ions/cm^2, compared to the as grown (25 Oe) and after AAO mask transfer (35 Oe) for the same sample. For comparison, we irradiated an LSMO sample without AAO masking with the same dose as sample S3. The irradiation effects on the LSMO sample showed a 370 Oe enhancement coercivity and no exchange bias (not shown). With increasing irradiation the hysteresis loop shapes become more rounded and the squareness (M_s/M_r) decreases (Fig. 5). This large coercive field enhancement appears only after the irradiation and is accompanied by a negative horizontal loop shift, i.e. exchange bias. For the highest dose irradiated sample, 151 Oe exchange bias field is measured after 1 kOe field cooling to 5 K. So the AAO mask transfer slightly decreases the total magnetization without changing the ferromagnetic transition temperature, whereas irradiation decreases the transition temperature considerably, produces a large coercive field enhancement and develops exchange bias.

Oxygen ion irradiation through the AAO mask imprints the nanoscale pattern into the LSMO thin films and can change the local magnetic ordering and induce spatially modulated order–disorder regions. The long range exchange interaction between these regions may cause loop shift and coercivity enhancement [38]. Within the ferromagnetic layer, defects alter the magnetic domain structure, leading to pinning sites for ferromagnetic domain walls. Immobilizing domain walls caused by their interaction with defects results in the suppression of the switching ability of a magnetic domain which results in a coercivity enhancement. An interfacial phase separation leading to additional pining centers may also contribute to the coercivity enhancement [39].

In addition to the structural defects, oxygen ion irradiation can induce chemical reordering, nanocrystallites or grain boundaries within the bombarded regions. Increased oxygen deficiency in LSMO thin films leads to a negative electric charge deficiency which is compensated by a Mn^{4+} decrease to keep charge neutrality. Therefore, increasing or decreasing oxygen content also affects the Mn^{4+}/Mn^{3+} ratio. Thus the mixed Mn valence can be changed by the oxygen depletion [36,40]. The presence of a large exchange bias field with enhanced coercivity for irradiated samples, but absence of exchange bias for the as-grown sample implies that the chemical composition and/or stoichiometry of the interfacial layers are different between bombarded and non-

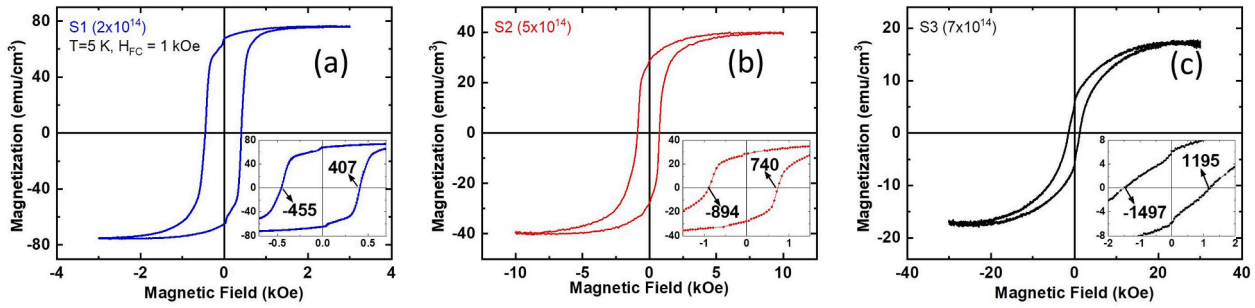

Fig. 5. Hysteresis loops for three different irradiation doses (a) 2×10^{14}, (b) 5×10^{14}, and (c) 7×10^{14} ions/cm^2. The curves were obtained using the same experimental protocol at 5 K after 1 kOe field cooling. Insets show a magnified view of the low field regions for the same curves for clarity.

Table 1
List of coercive field, exchange bias field, and magnetization values for as grown and after irradiation. All values were obtained from hysteresis measurements at 5 K after 1 kOe FC. Exchange bias fields obtained from hysteresis loops after diamagnetic correction for S1, S2, and S3 at maximum applied field of 3 kOe, 10 kOe, and 30 kOe, respectively.

Samples	Irradiation Dose (ions/cm^2)	AAO Pore Size (nm)	T_C (K)	After 1 kOe FC @ 5 K						
				As Grown		Irradiated				
				H_c (Oe)	H_{EB} (Oe)	H_{c1} (Oe)	H_{c2} (Oe)	H_C (Oe)	H_{EB} (Oe)	M_r/M_S
S1	2×10^{14}	70	283	26	–	−455	407	431	24	0.89
S2	5×10^{14}	70	228	22	–	−894	740	817	77	0.73
S3	7×10^{14}	70	123	25	–	−1497	1195	1346	151	0.35

bombarded regions. The interfacial layer could be due to the formation of Mn-rich oxide phases [41]. In the present case, the formation of interfacial antiferromagnetic phases, such as Mn or MnO, could give rise to the observed exchange bias, whereas the enhanced coercive field could result due to the formation of harder ferrimagnetic phases like Mn_3O_4 [42].

This scenario is further supported by the large coercive field enhancement and development of pronounced exchange bias below 50 K (Fig. 4). This indicates that a different mechanism operate below this temperature. Mn_3O_4 in bulk form is ferrimagnetic below 43 K transition temperature [43] while Mn_3O_4 nanocrystallites exhibit a reduced ferrimagnetic transition at 39 K [44]. Cluster size effects or surface spin effects in binary manganese oxides can result in various magnetic configurations. Antiferromagnetic MnO ($T_N = 118$ K [45]) nanoclusters in diameters of 5–10 nm show a ferromagnetic behavior below 27 K [46]. Therefore, below these critical temperatures, exchange interactions between the ferromagnetic host and formed interfacial antiferromagnetic phases can give rise to the exchange bias and coercive field enhancement.

The lateral and in-depth domain landscape of a ferromagnet and an antiferromagnet strongly influence the exchange bias and should be considered to understand the irradiation dose dependence (Fig. 4 inset). The exchange bias field increases with the number of uncompensated moments and crucially depends on the type of defects created, i.e., pinned or unpinned uncompensated magnetization [25]. Magnetic defects near the interface increase the area density of uncompensated moments which are expected to enhance the exchange bias field. In our system, the exchange couplings responsible for the observed bias occur throughout the entire volume of the film since internal interface structure, where ferromagnetic and antiferromagnetic couplings between atoms coexist, spatially distributed.

The induced exchange coupling in our samples depends of the maximum applied field. For sample S3, the exchange bias field decreases from 151 Oe to 59 Oe with increasing maximum applied field from 30 kOe to 90 kOe (not shown). Applying higher fields drags more and more pinned uncompensated magnetic moments along the field direction producing a lower exchange bias shift and higher remanence. The change in the anisotropy, corresponding magnetic phases induced upon bombardment, and field dependence of exchange bias needs further study.

5. Conclusion

In summary, a combination of oxygen ion irradiation and porous alumina mask was used to induce nano-structured defects on manganite thin films. The magnetic properties of the samples before and after the irradiation were compared. The irradiation reduces the ferromagnetic ordering temperature and total magnetization in addition to producing a large coercivity enhancement and develops exchange bias below 50 K. The experimental observations can be understood considering the ion irradiation induced defects in spatially confined regions that may lead to pinning sites for the ferromagnetic domain walls. Formation of Mn rich antiferromagnetic or ferrimagnetic phases within the bombarded regions that are exchange coupled to the ferromagnetic host could give rise to the loop shifts. These findings show that magnetic properties of complex oxide ferromagnets can be engineered by a combination of ion irradiation and AAO mask techniques.

CRediT authorship contribution statement

Ali C. Basaran: Conceptualization, Methodology, Investigation, Validation, Writing – original draft, Writing – review & editing. **C. Monton:** Conceptualization, Methodology, Investigation, Writing – review & editing. **J. Trastoy:** Software, Investigation. **R. Bernard:** Software, Investigation. **K. Bouzehouane:** Software, Investigation. **J.E. Villegas:** Conceptualization, Writing – review & editing. **Ivan K. Schuller:** Supervision, Writing – review & editing.

Declaration of Competing Interest

The authors declare that they have no known competing financial interests or personal relationships that could have appeared to influence the work reported in this paper.

Acknowledgements

We thank to M. Fitzsimmons for useful discussions. Work funded by the Department of Energy's Office of Basic Energy Science, DMR under grant DE FG02 87ER-45332. Work at CNRS-Thales funded by ERC 647100 "SUSPINTRONICS". Ali C. Basaran gratefully acknowledges Carnegie Mellon University's Courtesy Appointment as a fellow in its Distance Fellows Program in association with the Committee on Human Rights of the National Academy of Sciences, National Academy of Engineering, and National Academy of Medicine.

References

[1] M. Bowen, M. Bibes, A. Barthélémy, J.-P. Contour, A. Anane, Y. Lemaître, A. Fert, Appl. Phys. Lett. 82 (2003) 233.
[2] A. Urushibara, Y. Moritomo, T. Arima, A. Asamitsu, G. Kido, Y. Tokura, Phys. Rev. B: Condens. Matter 51 (1995) 14103.
[3] N.V. Volkov, Physics-Uspekhi 55 (2012) 250.
[4] M. Bibes, J.E. Villegas, A. Barthélémy, Adv. Phys. 60 (2011) 5.
[5] J.F. Mitchell, D.N. Argyriou, C.D. Potter, D.G. Hinks, J.D. Jorgensen, S.D. Bader, Phys. Rev. B: Condens. Matter 54 (1996) 6172.
[6] F. Tsui, M.C. Smoak, T.K. Nath, C.B. Eom, Appl. Phys. Lett. 76 (2000) 2421.
[7] J. Rhensius, C.A.F. Vaz, A. Bisig, S. Schweitzer, J. Heidler, H.S. Körner, A. Locatelli, M.A. Niño, M. Weigand, L. Méchin, F. Gaucher, E. Goering, L.J. Heyderman, M. Kläui, Appl. Phys. Lett. 99 (2011), 062508.
[8] Å. Monsen, J.E. Boschker, F. Macià, J.W. Wells, P. Nordblad, A.D. Kent, R. Mathieu, T. Tybell, E. Wahlström, J. Magn. Magn. Mater. 369 (2014) 197.
[9] M. Sirena, A. Zimmers, N. Haberkorn, E.E. Kaul, L.B. Steren, J. Lesueur, T. Wolf, Y. Le Gall, J.J. Grob, G. Faini, Phys. Rev. B: Condens. Matter 81 (2010), 134439.
[10] A. Gupta, G.Q. Gong, G. Xiao, P.R. Duncombe, P. Lecoeur, P. Trouilloud, Y. Y. Wang, V.P. Dravid, J.Z. Sun, Phys. Rev. B: Condens. Matter 54 (1996) R15629.
[11] E. Dagotto, T. Hotta, A. Moreo, Phys. Rep. 344 (2001) 1.
[12] F. Hellman, A. Hoffmann, Y. Tserkovnyak, G.S.D. Beach, E.E. Fullerton, C. Leighton, A.H. MacDonald, D.C. Ralph, D.A. Arena, H.A. Dürr, P. Fischer, J. Grollier, J.P. Heremans, T. Jungwirth, A.V. Kimel, B. Koopmans, I.N. Krivorotov, S.J. May, A.K. Petford-Long, J.M. Rondinelli, N. Samarth, I.K. Schuller, A.N. Slavin, M.D. Stiles, O. Tchernyshyov, A. Thiaville, B.L. Zink, Rev. Mod. Phys. 89 (2017), 025006.
[13] A.C. Basaran, T. Saerbeck, J. de la Venta, H. Huckfeldt, A. Ehresmann, I.K. Schuller, Appl. Phys. Lett. 105 (2014), 072403.
[14] J.G. Ramirez, T. Saerbeck, S. Wang, J. Trastoy, M. Malnou, J. Lesueur, J.-P. Crocombette, J.E. Villegas, I.K. Schuller, Phys. Rev. B: Condens. Matter 91 (2015), 205123.
[15] J. Trastoy, M. Malnou, C. Ulysse, R. Bernard, N. Bergeal, G. Faini, J. Lesueur, J. Briatico, J.E. Villegas, Nat. Nanotechnol. 9 (2014) 710.
[16] C. Chappert, H. Bernas, J. Ferré, V. Kottler, J.-P. Jamet, Y. Chen, E. Cambril, T. Devolder, F. Rousseaux, V. Mathet, H. Launois, Science 280 (1998) 1919.
[17] J. Fassbender, D. Ravelosona, Y. Samson, J. Phys. D: Appl. Phys. 37 (2004) R179.
[18] Ł. Frąckowiak, P. Kuświk, G.D. Chaves-O'Flynn, M. Urbaniak, M. Matczak, P. P. Michałowski, A. Maziewski, M. Reginka, A. Ehresmann, F. Stobiecki, Phys. Rev. Lett. 124 (2020), 047203.
[19] A.V. Krasheninnikov, K. Nordlund, J. Appl. Phys. 107 (2010), 071301.
[20] A. Ehresmann, Recent Res. Devel. Appl. Phys. 7 (2004) 401.
[21] Y. Takamura, R.V. Chopdekar, A. Scholl, A. Doran, J.A. Liddle, B. Harteneck, Y. Suzuki, Nano Lett. 6 (2006) 1287.
[22] M. Krupinski, R. Bali, D. Mitin, P. Sobieszczyk, J. Gregor-Pawlowski, A. Zarzycki, R. Böttger, M. Albrecht, K. Potzger, M. Marszałek, Nanoscale 11 (2019) 8930.
[23] G.E.J. Poinern, N. Ali, D. Fawcett, Materials 4 (2011) 487.
[24] Y.-K. Tang, Y. Sun, Z.-H. Cheng, Phys. Rev. B: Condens. Matter 73 (2006), 174419.
[25] J. Nogués, I.K. Schuller, J. Magn. Magn. Mater. 192 (1999) 203.
[26] T. Blachowicz, A. Ehrmann, Coatings 11 (2021) 122.
[27] T. Saerbeck, F. Klose, D. Lott, G.J. Mankey, Z. Lu, P.R. LeClair, W. Schmidt, A.P. J. Stampfl, S. Danilkin, M. Yethiraj, A. Schreyer, Phys. Rev. B: Condens. Matter 82 (2010), 134409.
[28] M. Ali, P. Adie, C.H. Marrows, D. Greig, B.J. Hickey, R.L. Stamps, Nat. Mater. 6 (2007) 70.
[29] J.-V. Kim, R.L. Stamps, Appl. Phys. Lett. 79 (2001) 2785.
[30] J. Guiliani, J. Cadena, C. Monton, Nanotechnology 29 (2018), 075301.
[31] J. Ziegler, J. Biersack, in: Treatise on Heavy-Ion Science, Springer, US, 1985, p. 93.
[32] L. Balcells, L. Abad, H. Rojas, B. Martínez, Nanotechnology 19 (2008), 135307.
[33] J.E. Villegas, I. Swiecicki, R. Bernard, A. Crassous, J. Briatico, T. Wolf, N. Bergeal, J. Lesueur, C. Ulysse, G. Faini, X. Hallet, L. Piraux, Nanotechnology 22 (2011), 075302.
[34] S.W. Shin, S.G. Lee, J. Lee, C.N. Whang, J.H. Lee, I.H. Choi, T.G. Kim, J.H. Song, Nanotechnology 16 (2005) 1392.
[35] M.L. Wilson, J.M. Byers, P.C. Dorsey, J.S. Horwitz, D.B. Chrisey, M.S. Osofsky, J. Appl. Phys. 81 (1997) 4971.
[36] R. Cauro, A. Gilabert, J.P. Contour, R. Lyonnet, M.G. Medici, J.C. Grenet, C. Leighton, I.K. Schuller, Phys. Rev. B: Condens. Matter 63 (2001), 174423.
[37] A.M. De Léon-Guevara, P. Berthet, J. Berthon, F. Millot, A. Revcolevschi, A. Anane, C. Dupas, K. Le Dang, J.P. Renard, P. Veillet, Phys. Rev. B: Condens. Matter 56 (1997) 6031.
[38] J. Juraszek, J. Fassbender, S. Poppe, T. Mewes, B. Hillebrands, D. Engel, A. Kronenberger, A. Ehresmann, H. Schmoranzer, J. Appl. Phys. 91 (2002) 6896.
[39] M. Sharma, J. Gazquez, M. Varela, J. Schmitt, C. Leighton, Phys. Rev. B: Condens. Matter 84 (2011), 024417.
[40] D. Schumacher, A. Steffen, J. Voigt, J. Schubert, T. Brückel, H. Ambaye, V. Lauter, Phys. Rev. B: Condens. Matter 88 (2013), 144427.
[41] L. Poggini, S. Ninova, P. Graziosi, M. Mannini, V. Lanzilotto, B. Cortigiani, L. Malavolti, F. Borgatti, U. Bardi, F. Totti, I. Bergenti, V.A. Dediu, R. Sessoli, J. Phys. Chem. C 118 (2014) 13631.
[42] I. Bergenti, P.K. Manna, C.-H. Lin, P. Graziosi, X. Liu, G.L. Causer, F. Liscio, A. Ruotolo, V.A. Dediu, J.v. Lierop, F. Klose, K.-W. Lin, J. Appl. Phys. 124 (2018), 183903.
[43] B. Boucher, R. Buhl, M. Perrin, J. Appl. Phys. 42 (1971) 1615.
[44] I.K. Gopalakrishnan, N. Bagkar, R. Ganguly, S.K. Kulshreshtha, J. Cryst. Growth 280 (2005) 436.
[45] C.G. Shull, W.A. Strauser, E.O. Wollan, Phys. Rev. 83 (1951) 333.
[46] G.H. Lee, S.H. Huh, J.W. Jeong, B.J. Choi, S.H. Kim, H.-C. Ri, J. Am. Chem. Soc. 124 (2002) 12094.